

Magneto-intersubband resistance oscillations in GaAs quantum wells placed in a tilted magnetic field.

William Mayer, Jesse Kanter, Javad Shabani, and Sergey Vitkalov*
Physics Department, City College of the City University of New York, New York 10031, USA

A. K. Bakarov
A.V.Rzhanov Institute of Semiconductor Physics, Novosibirsk 630090, Russia

A. A. Bykov
A.V.Rzhanov Institute of Semiconductor Physics, Novosibirsk 630090, Russia and
Novosibirsk State University, Novosibirsk 630090, Russia
(Dated: November 23, 2021)

The magnetotransport of highly mobile 2D electrons in wide GaAs single quantum wells with three populated subbands placed in titled magnetic fields is studied. The bottoms of the lower two subbands have nearly the same energy while the bottom of the third subband has a much higher energy ($E_1 \approx E_2 \ll E_3$). At zero in-plane magnetic fields magneto-intersubband oscillations (MISO) between the i^{th} and j^{th} subbands are observed and obey the relation $\Delta_{ij} = E_j - E_i = k \cdot \hbar\omega_c$, where ω_c is the cyclotron frequency and k is an integer. An application of in-plane magnetic field produces dramatic changes in MISO and the corresponding electron spectrum. Three regimes are identified. At $\hbar\omega_c \ll \Delta_{12}$ the in-plane magnetic field increases considerably the gap Δ_{12} , which is consistent with the semi-classical regime of electron propagation. In contrast at strong magnetic fields $\hbar\omega_c \gg \Delta_{12}$ relatively weak oscillating variations of the electron spectrum with the in-plane magnetic field are observed. At $\hbar\omega_c \approx \Delta_{12}$ the electron spectrum undergoes a transition between these two regimes through magnetic breakdown. In this transition regime MISO with odd quantum number k terminate, while MISO corresponding to even k evolve *continuously* into the high field regime corresponding to $\hbar\omega_c \gg \Delta_{12}$.

I. INTRODUCTION

The quantization of electron motion in magnetic fields generates a great variety of fascinating phenomena observed in condensed materials. A well-known example is the Shubnikov-de Haas (SdH) resistance oscillations¹. The passage of strongly degenerate Landau levels through the Fermi surface at a low temperature T produces resistance oscillations due to a modulation of the net number of electron states in the energy interval $kT < \hbar\omega_c$ near the Fermi energy E_F that provide the dominant contribution to electron transport^{2,3}. In two dimensional electron systems, SdH oscillations can be very pronounced², leading to the Quantum Hall Effect (QHE) at low temperatures $kT \ll \hbar\omega_c$ ⁴.

Landau quantization produces a remarkable effect on Joule heating of two dimensional (2D) electrons⁵⁻⁸. The heating forces 2D electrons into exotic electronic states in which voltage (current) does not depend on current⁹⁻¹¹ (voltage¹²). In contrast to the linear response at low temperatures $kT < \hbar\omega_c$ (SdH, QHE), the quantization affects Joule heating in a significantly broader temperature range. At $kT \gg \hbar\omega_c$ the *dc* heating produces a multi-tiered electron distribution containing as many tiers as the number of Landau levels inside the energy interval kT : $N \approx kT/\hbar\omega_c$. This quantal heating preserves the overall broadening ($\sim kT$) of the electron distribution^{7,13}. Surprisingly the electron distribution resulting from quantal heating is, in some respect, similar to the one created by quantum microwave pumping be-

tween Landau levels^{15,16}. Indicated phenomena produce a broad variety of nonlinear effects in quantizing magnetic fields and present an exciting area of contemporary research¹⁴.

Two-dimensional electron systems with multiple populated subbands exhibit additional quantum magnetoresistance oscillations¹⁷⁻²⁴. These magneto-inter-subband oscillations (MISO) of the resistance are due to an alignment between Landau levels from different subbands i and j with corresponding energies E_i and E_j . Resistance maxima occur at magnetic fields at which the gap between the bottoms of subbands, $\Delta_{ij} = E_i - E_j$, equals a multiple of the Landau level spacing, $\hbar\omega_c$: $\Delta_{ij} = k \cdot \hbar\omega_c$, where k is an integer²⁵⁻²⁸. At this condition electron scattering on rigid impurities is enhanced due to the possibility of electron transitions between i^{th} and j^{th} subbands. At magnetic fields corresponding to the condition $\Delta_{ij} = (k + 1/2) \cdot \hbar\omega_c$ the intersubband electron transitions are suppressed. As a result, the resistance oscillations are periodic in inverse magnetic field due to this modulation of electron scattering. In contrast to SdH oscillations MISO are less sensitive to temperature. MISO are observed at temperatures, $kT \gg \hbar\omega_c$ at which SdH oscillations (and QHE) are absent.

This paper presents investigations of MISO in wide quantum wells with three populated subbands placed in a tilted magnetic field. Studied systems contain conducting electrons localized near the edges of the quantum wells. The electrons, thus, form two parallel 2D systems separated by a distance d . A weak electron tunneling

between these two systems occurs through a relatively wide but shallow potential. In zero magnetic field the lateral (along 2D systems) and vertical (between 2D systems) motions of an electron are completely disentangled. The vertical tunneling uniformly splits the electron spectrum originally degenerate in the lateral directions. The resulting eigenvalues correspond to symmetric (E_1) and antisymmetric (E_2) configurations of electron wave functions in the vertical direction with the energy gap $\Delta_{12} = E_2 - E_1$ between two subbands independent of the lateral wave vector \vec{k} .

The bottom of the third subband has a much higher electron energy $E_3 \gg E_{1,2}$. Application of perpendicular magnetic field quantizes the lateral motion in all subbands inducing MISOs. The MISOs corresponding to electron scattering between the third and the two lower subbands oscillate at high frequencies and demonstrate a distinct beating pattern. This useful property provides a very accurate measurement of the evolution of the electron spectrum in response to in-plane magnetic field.

Application of in-plane magnetic field couples the symmetric and antisymmetric states^{29,30} leading to a significant modification of the electron spectrum. Theoretical investigations of the electronic structure of two parallel 2D dimensional electron systems in tilted magnetic fields have revealed three regimes occurring at small ($\hbar\omega_c \ll \Delta_{12}$, semi-classical (SC) regime), strong ($\hbar\omega_c \gg \Delta_{12}$, high field (HF) regime) and intermediate (magnetic breakdown (MB) regime) magnetic fields³⁰. The intermediate magnetic fields correspond to magnetic breakdown³¹⁻³⁴ of the semi-classical electron spectrum leading generally to complex combinations of semi-classical orbits³⁴⁻³⁶. These regimes have been investigated to a different extent mainly in double quantum wells using SdH oscillations and QHE.^{29,37-40} However the results have not been compared coherently with the theory across all three regimes and important properties of the quantum oscillations have not been revealed. We note also that in the regime of QHE the energy spectrum is often sensitive to effects of the electrostatic redistribution of 2D carriers between different subbands and quantum levels, which makes a quantitative comparison between different regimes challenging^{42,43}.

This paper presents an attempt to study the evolution of the electron spectrum in wide quantum wells with in-plane magnetic field using MISO. The experiments are performed at a high temperature $kT \gg \hbar\omega_c$ at which effects of the electrostatic electron redistribution between Landau levels are, most likely, not relevant. The paper shows both MISO and SdH oscillations obtained at different angles α between the magnetic field and the normal to the 2D systems and yields a detailed evolution of electron spectrum in multi-subband 2D systems in a broad range of magnetic fields. Presented results show a termination of the MISO corresponding to $\Delta_{12} = k \cdot \hbar\omega_c$ at odd k in the magnetic breakdown regime. The termination is accompanied by a collapse of the nodes in the beating between MISOs corresponding to the third

subband. The obtained data demonstrate a good agreement with numerical simulations based on the existing theory³⁰ in a broad range of magnetic fields including all regimes indicated above.

Our experiments have revealed an outstanding sensitivity of the electron spectrum to the angle α , especially at $\hbar\omega_c \approx \Delta_{12}$. The sensitivity to in-plane magnetic field is due to both a strong Lorentz force, which occurs in studied samples with high electron density, and a weak tunneling between 2D parallel systems. The presented results indicate that the recently observed ambiguity in the MISO amplitude at $k=1$ is, most likely, related to a small misalignment between the direction of the magnetic field and the normal to 2D sample in different measurements^{44,45}.

II. EXPERIMENTAL SETUP

Studied GaAs quantum wells were grown by molecular beam epitaxy on a semi-insulating (001) GaAs substrate. The material was fabricated from a selectively doped GaAs single quantum well of width $d = 56$ nm sandwiched between AlAs/GaAs superlattice barriers. The heterostructure has three populated subbands with energies $E_1 \approx E_2 \ll E_3$ at the bottoms of the subbands. The subband energies are schematically shown in the insert to Figure 1.

The studied samples were etched in the shape of a Hall bar. The width and the length of the measured part of the samples are $W = 50\mu\text{m}$ and $L = 250\mu\text{m}$. AuGe eutectic was used to provide electric contacts to the 2D electron gas. Two samples were studied at temperature 4.2 Kelvin in magnetic fields up to 4 Tesla applied *in-situ* at different angle α relative to the normal to 2D layers and perpendicular to the applied current. The angle α has been evaluated using Hall voltage $V_H = B_{\perp}/(en_T)$, which is proportional to the perpendicular component, $B_{\perp} = B \cdot \cos(\alpha)$, of the total magnetic field B . The total electron density of samples, $n_T \approx 8.6 \times 10^{11} \text{cm}^{-2}$, was evaluated from the Hall measurements taken at $\alpha=0^\circ$ in classically strong magnetic fields³. An average electron mobility $\mu \approx 1.6 \times 10^6 \text{cm}^2/\text{Vs}$ was obtained from n_T and the zero-field resistivity. Sample resistance was measured using the four-point probe method. We applied a 133 Hz *ac* excitation $I_{ac}=1\mu\text{A}$ through the current contacts and measured the longitudinal and Hall *ac* voltages (V_{xx}^{ac} and V_H^{ac}) using two lockin amplifiers with 10M Ω input impedances. The potential contacts provided insignificant contribution to the overall response due to small values of the contact resistance (about 1k Ω) and negligibly small electric current flowing through the contacts. The measurements were done in the linear regime in which the voltages are proportional to the applied current.

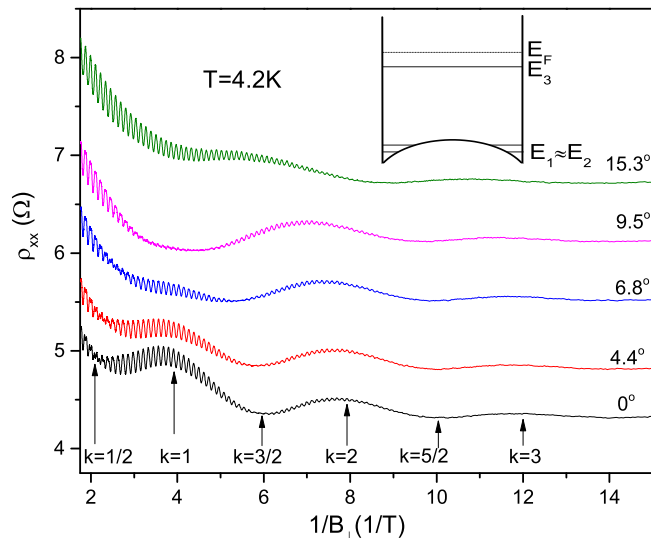


FIG. 1: (Color online) Dependencies of the longitudinal resistance ρ_{xx} on the inversed component of the magnetic field, which is perpendicular to the 2D sample, $1/B_{\perp}$, obtained at different angles α between the total magnetic field \vec{B} and the normal to the samples as labeled. Integer values of index k corresponds to the maximums of LF-MISO at $\Delta_{12} = k \cdot \hbar\omega_c$ (see Eq.(1)) and to anti-nodes of the beat pattern of HF-MISO. Half-integer value of k corresponds to the minimums of LF-MISO and the nodes of the HF-MISO beat pattern at angle $\alpha = 0^{\circ}$. Sample A. The insert presents the energy diagram of studied samples.

III. RESULTS AND DISCUSSION

A theoretical analysis yields the following expression for the amplitude of MISO due to the scattering between the i^{th} and j^{th} subbands in weak ($\omega_c\tau_q^{(i)} < 1$) perpendicular magnetic fields^{27,28}:

$$\Delta\rho_{MISO}^{(i,j)} = \frac{2m \cdot \nu_{ij}}{e^2(n_i + n_j)} \cdot \cos\left(\frac{2\pi\Delta_{ij}}{\hbar\omega_c}\right) \times \exp\left[\frac{-\pi}{\omega_c} \left(1/\tau_q^{(i)} + 1/\tau_q^{(j)}\right)\right], \quad (1)$$

where n_i and $\tau_q^{(i)}$ are the electron density and quantum scattering time⁴⁶ in the i^{th} subband, ν_{ij} is an effective intersubband transport scattering rate, m is the effective electron mass and $\omega_c = eB_{\perp}/m$ is the cyclotron frequency²⁸. This expression has recently been used in systems with two and three populated subbands to extract the quantum scattering rate $1/\tau_q^{i19-24,44,45}$. The expression indicates that MISO between i^{th} and j^{th} subbands are periodic in inverse magnetic field $1/B_{\perp}$.

Figure 1 presents the longitudinal resistivity, $\rho_{xx}(1/B_{\perp})$, of sample A at different angles α between the magnetic field and the normal to the sample as labeled. At $\alpha = 0^{\circ}$ in accordance with Eq.(1) the fre-

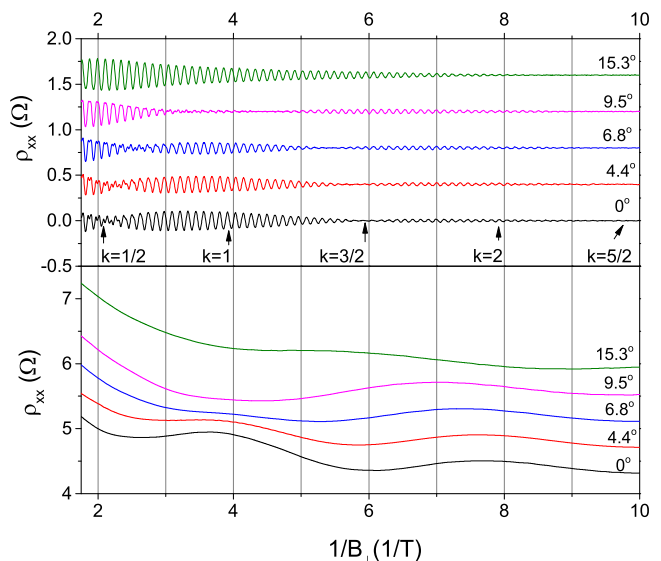


FIG. 2: (Color online) Lower (upper) panel presents LF-MISO (HF-MISO) obtained by a low (high) frequency FFT filtering of the magnetoresistance oscillations presented in Fig.1. Sample A.

quency of MISO in inverse magnetic field is proportional to the intersubband energy gap ($f_{ij} \propto \Delta_{ij} = E_i - E_j$). This three subband system should therefore have MISOs at three different frequencies, corresponding to resonant scattering between the subbands. MISOs associated with scattering between the two lowest subbands have a low frequency (LF-MISO), $f_{21} \propto E_2 - E_1$, since the energy gap Δ_{21} is very small ($E_1 \approx E_2$). The two sets of MISOs associated with scattering between the upper band and each of the lower bands have much higher frequencies, $f_{31} \approx f_{32} \gg f_{12}$ (HF-MISO), that are approximately equal since $\Delta_{31} \approx \Delta_{32} \gg \Delta_{21}$. Due to the small difference between energy E_1 and E_2 the interference between MISOs with frequencies f_{31} and f_{32} produces a beating pattern with a small beating frequency $f_{beat} \propto (E_2 - E_1)/2 \ll f_{3i}$ and a high inner frequency $f_+ \propto (2E_3 - E_2 - E_1)/2$. The resistance oscillations with both the low (f_{21}) and high (f_{31}, f_{32}) frequencies are shown in Figure 1.

The significant frequency difference between the low and high frequency contents of oscillations facilitates the separation of HF and LF-MISOs by fast Fourier transform (FFT) filtering. In Figure 2 the lower panel presents the low frequency content while the upper panel presents the high frequency oscillations, which have been filtered from the curves presented in Fig.1⁴⁵.

Due to the precise relation between different frequencies the beating frequency is half of the frequency of MISO corresponding to the two lower subbands: $f_{beat} = f_{21}/2$ at $\alpha=0^{\circ}$. This is indeed seen in Figure 2. Figures 1 and 2 show that at $\alpha=0^{\circ}$ the nodes of HF-MISO correspond to the minimums of the LF-MISO. Furthermore an analysis of the HF-MISO phase indicates that in the

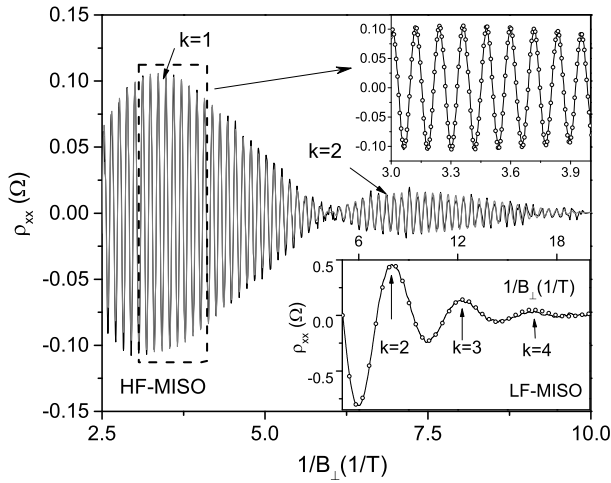


FIG. 3: Comparison of HF-MISO shown by the black solid line with the theoretical dependence based on Eq.(1) and shown by the gray line. Upper insert demonstrates a more detailed view of the comparison. Lower insert show a comparison of LF-MISO with the theory. In both inserts open circles present theoretical dependencies. Sample A.

$k=2$ region the phase of HF-MISO is shifted by π with respect to the HF-MISO phase in $k=1$ region at $\alpha=0^0$. To verify this π -phase shift, we compare HF-MISO at $\alpha=0^0$ with the one at $\alpha=15.3^0$, which demonstrates no nodes and is perfectly periodic with respect to $1/B_{\perp}$. The comparison shows that in the $k=1$ region the maximums of HF-MISO at $\alpha=0^0$ corresponds to the minimums of HF-MISO at $\alpha=15.3^0$, while in $k=2$ region the maximums of HF-MISO at $\alpha=0^0$ corresponds to the maximums of HF-MISO at $\alpha=15.3^0$. Thus the observed interference of HF-MISOs at $\alpha=0^0$ corresponds to the beating between two frequencies at $f_{beat} = f_{21}/2$.

Figure 3 demonstrates the direct comparison of HF-MISO at $\alpha=0^0$ with Eq.(1). The experiment agrees well with the theory in the whole range of magnetic fields corresponding to $\Delta_{12} > \hbar\omega_c$. At higher magnetic fields a quantitative comparison has not been accomplished due to the presence of SdH oscillations and higher harmonics of MISO, which are not captured in Eq.(1). Figure 3 presents also a comparison of LF-MISO with the theory. Shown in Fig.1 the monotonic background corresponding to the positive quantum magnetoresistance^{46,47} has been removed by a procedure reported earlier⁴⁵. However the relatively strong increase of the resistance observed at $\hbar\omega_c > \Delta_{12}$ interferes with the low frequency oscillating content making the applied procedure to be quite uncertain there. This comparison is limited to the magnetic fields corresponding to condition $k > 3/2$. In this range of magnetic fields a very good agreement between LF-MISO and the theory is found. A joint analysis of LF-MISO and HF-MISO yields the quantum scattering time in each subband⁴⁵. In lower subbands the time is found to be $\tau_q^{(1,2)} = 8.2 \pm 0.3$ ps while in the third subband the time is $\tau_q^{(3)} = 3.5 \pm 0.3$ ps. These values agree

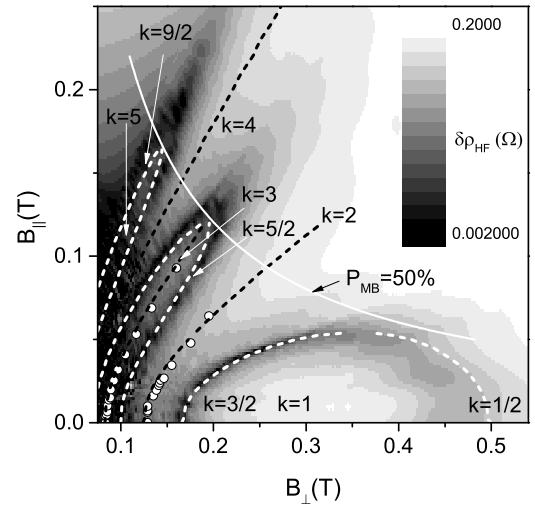


FIG. 4: Dependence of HF-MISO magnitude on B_{\perp} and B_{\parallel} . Black color presents locations of HF-MISO nodes. Open circles present experimental positions of LF-MISO maximums. White (black) dash lines present position of HF-nodes (LF-maximums) obtained using numerical calculations of electron spectrum. White solid line corresponds to 50% probability of magnetic breakdown of semi-classical trajectories³⁰. All spectra are obtained at $t_0=0.215$ meV and $d=36$ nm. Size of the circles corresponds to experimental uncertainty of the position. Sample A.

with those ones obtained in similar systems with three populated subbands⁴⁵.

An introduction of a parallel magnetic field, B_{\parallel} , produces significant changes in MISO. The most notable is the disappearance of the $k=1$ maximum, which occurs near angle $\alpha=9.5^0$ in Fig.2. This disappearance is accompanied by a spectacular collapse of two nodes of HF-MISO corresponding to $k=1/2$ and $k=3/2$ at $\alpha=0^0$. These nodes collapse in the vicinity of the main LF-MISO maximum $k=1$.

Figure 4 presents the evolution of the magnitude of HF-MISO in the $(B_{\perp}-B_{\parallel})$ plane. The HF-MISO magnitude (the envelop of HF-MISO) was obtained by a low frequency filtering of the square of HF-MISO: $\delta\rho_{HF} = (2\langle A^2 \cos^2(2\pi f_+/B_{\perp}) \rangle)^{1/2} = A$, where $A(B_{\perp}, B_{\parallel})$ is the slowly varying magnitude of HF-MISO and angle brackets stand for the low frequency filtering. The low pass filter rejects the high frequency content of the squared HF-MISO but passes slow oscillations at the beating frequency. The applied procedure yields the envelop of the HF-MISO with a standard deviation within $\pm 0.004\Omega$ ⁴⁸.

Figure 4 shows very different behavior of the odd and even MISO maximums in response to B_{\parallel} . The even ($k=2,4,\dots$) maximums of the MISO magnitude evolve continuously into the high magnetic field region, whereas the odd ($k=1,3,\dots$) maximums terminate within the regions bounded by HF-MISO nodes as shown in Figure 4. A transition from an odd region to an even region changes the phase of HF-MISO by π .

The figure demonstrates an additional interesting

MISO property in the B_{\perp} - B_{\parallel} plane: a possibility of the continuous (without intersection with a node line) transition between even maximums. Indeed by an appropriate choice of the B_{\perp} and B_{\parallel} the MISO maximum at $k=2$ can be transferred into $k=4$ MISO maximum at $\alpha=0^0$ without intersecting the nodal lines. In this sense all even maximums are topologically equivalent. This set also includes the $k=0$ maximum corresponding to the limit of strong magnetic fields. In contrast an odd MISO maximum presents an energy spectrum, which is topologically different from the spectrum corresponding to strong magnetic fields. The latter is the spectrum of uncoupled 2D systems^{1,30}.

A. Numerical analysis of electron spectrum

The evolution of MISO with both in-plane and perpendicular magnetic fields is found to be in good agreement with numerical evaluations of the electron spectrum in those field⁴⁹. In this section we present a theory describing the effect of in-plane magnetic field on the electron spectrum of two 2D parallel electron systems^{30,41}. The theory treats the interlayer hopping in a tight binding approximation so that the single-particle problem is characterized by the interlayer distance d and hopping integral t_0 ³⁰. In the titled magnetic field $\vec{B} = (-B_{\parallel}, 0, B_{\perp})$ electrons are described by the Hamiltonian:

$$H = \frac{\hbar^2 k_x^2}{2m^*} + \frac{e^2 B_{\perp}^2}{2m^*} x^2 + \frac{\hbar^2 k_z^2}{2m^*} + V(z) + \frac{e^2 B_{\parallel}^2}{2m^*} z^2 + \frac{e^2 B_{\perp} B_{\parallel}}{m^*} xz, \quad (2)$$

where m^* is effective mass and $V(z)$ is the electrostatic potential between two 2D systems. To obtain Eq.(2) we have used the gauge $(0, B_{\perp}x + B_{\parallel}z, 0)$ of the vector potential and applied the transformation $x \rightarrow x - \hbar k_y / e B_{\perp}$.

The first four terms describe the coupled 2D electron systems in a perpendicular magnetic field. The corresponding eigenfunctions of the system are $|N, \xi\rangle$, where $N=0,1,2..$ presents N -th Landau level (the lateral quantization) and $\xi = S, AS$ describes the symmetric (S) and antisymmetric (AS) configurations of the wave function in the z -direction (vertical quantization). Using functions $|N, \xi\rangle$ as the basis set, one can present the Hamiltonian in matrix form. The matrix contains four matrix blocks: $\hat{H} = (\hat{E}^S, \hat{T}; \hat{T}, \hat{E}^{AS})$, where the semicolon separates rows. The diagonal matrices, \hat{E}^S and \hat{E}^{AS} , represent energy of the symmetric and antisymmetric wave functions in different orbital states N :

$$E_{mn}^{S,AS} = \delta_{mn} [\hbar\omega_c ((n-1) + \frac{1}{2}) \pm t_0 + \frac{e^2 B_{\parallel}^2 d^2}{8m^*}], \quad (3)$$

where sign $-(+)$ corresponds to symmetric (antisymmetric) states and indexes $m=1,2..N_{max}$ and $n=1,2..N_{max}$ numerate rows and columns of the matrix correspondingly. These indexes are related to the orbital number N : $n, m = N + 1$, since the orbital number $N = 0, 1, 2..$ In numerical computations the maximum number N_{max}

is chosen to be about twice larger than the orbital number N_F corresponding to Fermi energy E_F . Further increase of N_{max} show a very small (within 1%) deviation from the dependencies obtained at $N_{max} \approx 2N_F$.

The first term in Eq.(3) describes the orbital quantization of electron motion while the second term relates to the electron tunneling between 2D layers. The shape of the wave function in the z -direction ($\xi(z)$) is determined by the third and fourth terms in Eq.(2). Due to the complete disentanglement between the vertical (z) and lateral motions at $B_{\parallel}=0$ T the second term does not depend on N . The tunneling term reads: $\langle \xi | V(z) | \xi \rangle = \pm t_0$. In the tight binding approximation t_0 is considered to be independent of B_{\parallel} ³⁰. As shown below this approximation provides very good agreement with experiment. The last term in Eq.(3) describes diamagnetic shift of the quantum levels and is related to the fifth term in Eq.(2). In the basis set $|N, \xi\rangle$ the diamagnetic term is proportional to $\langle \xi | z^2 | \xi \rangle = (d/2)^2$, since in the tight binding approximation the thin 2D layers are located at distance $z = \pm d/2$ from the origin of z axes. The diamagnetic term does not depend on N .

The off-diagonal matrix \hat{T} is related to the last term in Eq.(2), which mixes symmetric and antisymmetric states. Since $x = l_{B\perp}(a^* + a)/\sqrt{2}$ works as the raising a^* and lowering a operators of the Landau orbits, the last term in Eq.(2) couples Landau levels with orbital numbers different by one. Here $l_{B\perp} = (\hbar/eB_{\perp})^{1/2}$ is the magnetic length in B_{\perp} . As a result, for $n > m$ the matrix element T_{mn} between states $|N, S\rangle$ and $|N + 1, AS\rangle$ is

$$\begin{aligned} T_{mn} &= \delta_{m+1,n} \frac{e^2 B_{\parallel} B_{\perp} l_{B\perp}}{m^*} \langle N | \frac{a^* + a}{\sqrt{2}} | N + 1 \rangle \langle S | z | AS \rangle \\ &= \delta_{m+1,n} \hbar\omega_c \left[\frac{B_{\parallel} d}{2B_{\perp} l_{B\perp}} \right] (n/2)^{1/2} \end{aligned} \quad (4)$$

The matrix \hat{T} is a symmetric matrix: $T_{mn} = T_{nm}$. The Hamiltonian \hat{H} is diagonalized numerically at different magnetic fields B_{\perp} and B_{\parallel} . To analyze the spectrum the obtained eigenvalues of the Hamiltonian are numerated in ascending order using positive integer index $l=1,2,...$ The electron transport depends on the distribution of the quantum levels in the interval kT near the Fermi energy E_F ³. Below we focus on this part of the spectrum.

In accordance with Eq.(1) a HF-node corresponds to an equal separation ($\hbar\omega_c/2$) between nearest quantum levels in the vicinity of Fermi energy, whereas a HF-anti-node occurs when the two nearest levels coincide with each other, thus, the energy separation between pairs of coinciding levels is $\hbar\omega_c$. We note, that, in contrast to the nodes of HF-MISO, the positions of the maximums of the magnitude of HF-MISO and maximums of LF-MISO, shown in Fig.1 and Fig.3, are affected by the Dingle factor and, therefore, do not exactly correspond to the magnetic fields at which two nearest Landau levels coincides. In accordance with Eq.(1) the exponential decrease of the Dingle factor reduces significantly the beating magnitude

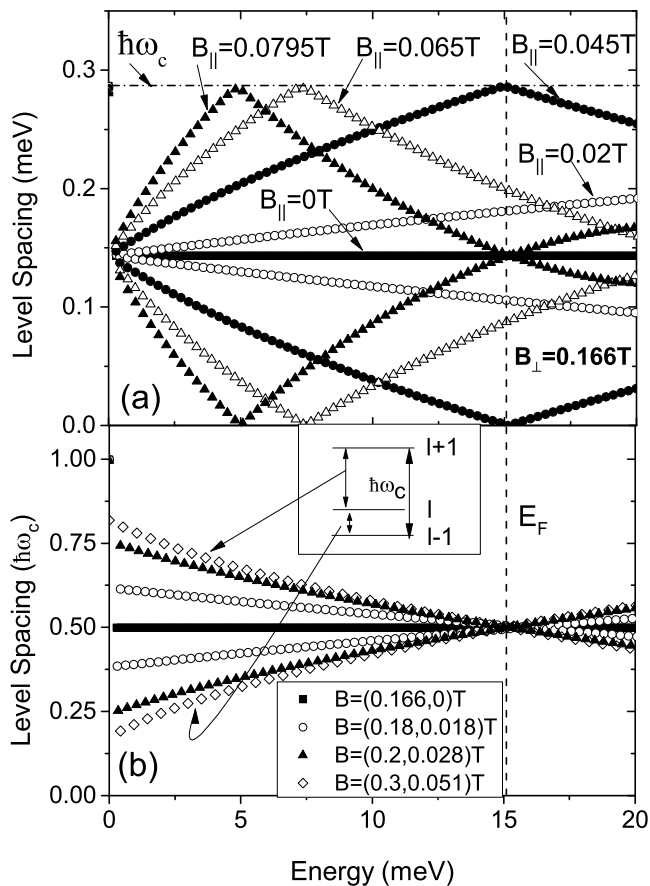


FIG. 5: (a) Level spacing $\delta E_l = E_{l+1} - E_l$ in the energy spectrum of electrons in fixed $B_{\perp} = 0.166$ T at different in-plane magnetic fields as labeled. At $B_{\parallel} = 0$ T the quantum levels are equally spaced with the energy separation $\delta E_l = \hbar\omega_c/2$ producing $k=3/2$ HF-MISO node. At a finite in-plane field the level spacing depends on the energy leading to $k=2$ HF-MISO anti-node at $B_{\parallel} = 0.045$ T and $k=5/2$ HF-node at $B_{\parallel} = 0.0795$ T; (b) Level spacing $\delta E_l = E_{l+1} - E_l$ in the energy spectrum at different B_{\perp} and B_{\parallel} magnetic fields as labeled. These fields correspond to the nodal line between $k=3/2$ and $k=1/2$ HF-nodes shown in Fig.4. The insert explains the meaning of the upper and lower branches of the energy dependence of the level spacing. All spectra are obtained at $t_0 = 0.215$ meV and $d = 36$ nm.

at small magnetic fields and, thus, shifts the maximums of the beating pattern to higher magnetic fields. Figures 1 and 2 indicate that the shift is more pronounced for maximums of magnitude of HF-MISO (in comparison with the maximums of LF-MISO) due to the considerably shorter quantum electron lifetime, $\tau_q^{(3)}$, and, thus, stronger effect of the Dingle factor in the third subband.

Figure 5(a) presents the difference between energies of $l+1$ -th and l -th quantum levels of the full electron spectrum obtained in the perpendicular magnetic field $B_{\perp} \approx 0.166$ T at different in-plane magnetic fields as labeled. Each symbol represents a particular level spacing: $\delta E_l = E_{l+1} - E_l$. At $B_{\parallel} = 0$ and $B_{\perp} \approx 0.166$ T the electron spectrum corresponds to the $k=3/2$ HF-MISO node and

the LF-MISO minimum. At this node the level spacing $\delta E_l = \hbar\omega_c/2 \approx 14$ meV is the same for all quantum levels except the first two lowest levels, which are separated by $\hbar\omega_c$.

Due to the complete separation between the lateral and vertical electron motions at $B_{\parallel} = 0$ the level spacing is independent on energy for any B_{\perp} . However in general the level spacing contains two branches corresponding to the nearest upper and lower neighbors of a quantum level. This is shown in the insert to Fig.5(b). In the case of a node at $B_{\parallel} = 0$ T these two branches coincide everywhere, while for a node at a finite B_{\parallel} the two branches intersect in the vicinity of the Fermi energy. The numeric evaluation of the spectrum indicates also that the level spacing does not exceed the cyclotron energy $\hbar\omega_c$ and maintains the periodicity of the spectrum $\delta E_{l+1} + \delta E_l = \hbar\omega_c$. This is related to the fact that the Hamiltonian \hat{H} is independent on k_y , which preserves the degeneracy of quantum levels, $g = 1/(2\pi l_{\perp}^2)$, in in-plane magnetic fields.³⁰

Application of an in-plane magnetic field couples the vertical and lateral degrees of freedom. This causes the distribution of level spacing to be energy dependent. The B_{\parallel} -coupling is due the Lorent's force and, thus, increases with the electron velocity (energy). At the bottom of a subband the B_{\parallel} -coupling is small and the spectrum is nearly preserved. At $B_{\parallel} = 0.02$ T the level spacing spreads out almost linearly with the energy. At a higher in-plane field $B_{\parallel} = 0.045$ T the spread of the level distribution reaches a maximum $\hbar\omega_c$ in the vicinity of E_F . At this condition the two nearest quantum levels coincide with each other. This is the $k=2$ maximum of HF-MISO magnitude and LF-MISO shown in Fig.4. Further increase of the in-plane field decreases the spread of the level distribution and in the vicinity of Fermi energy the electron spectrum gradually evolves into a state with nearly uniform level distribution at $B_{\parallel} = 0.0795$ T (intersection of two branches). It corresponds to $k=5/2$ node shown in Fig.4. At this magnetic field variations of the level spacing is nonlinear with the energy.

Figure 5(b) presents the level spacing δE_l obtained at different perpendicular and in-plane magnetic fields as labeled. These fields corresponds to the HF-node $k=3/2$. The figure shows that an increase of the in-plane magnetic field shifts the $k=3/2$ node to a higher perpendicular magnetic field. At small B_{\parallel} this behavior corresponds to the semi-classical regime and is described below.

The numerically obtained evolution of the HF-nodes and LF-maximums in the $B_{\perp} - B_{\parallel}$ plane is shown in Figure 4. A good overall agreement between experiment and the theory is found. A statistical analysis of the experimental and theoretical positions of HF-nodes indicates the standard deviation below 0.002 T for the $k=3/2$ HF-MISO node in the range $B_{\perp} \in (0.15-0.35)$ T. The standard deviation between experiment and theory in the vicinity of the $k=1/2$ node ($B_{\perp} \in (0.35-0.5)$ T) is found to be significantly larger (0.02 T). In this region the experimental data deviates systematically from the theory. The experimental and theoretical node positions around the $k=3$

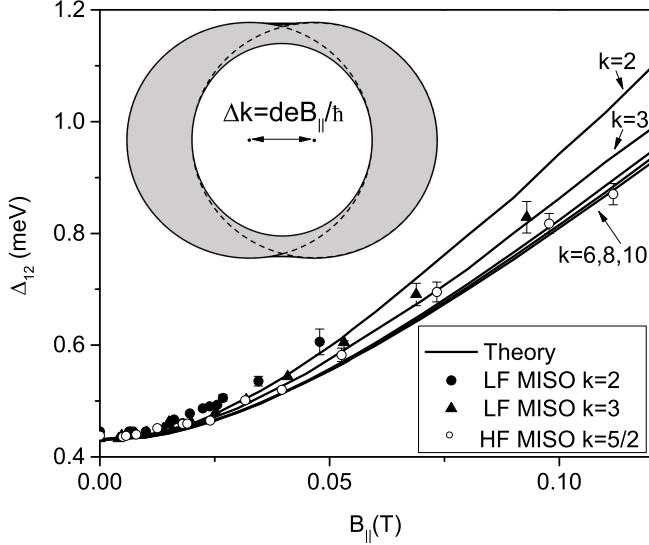


FIG. 6: Dependence of the gap Δ_{12} on in-plane magnetic field extracted from positions of LF-MISO maximums and a HF-MISO node as labeled. Solid lines represent the gap obtained from the electron spectra evaluated numerically at $t_0=0.215$ meV and $d=36$ nm for different LF-MISO maximums as labeled. For $k=2, 3$ and $5/2$ standard deviations between experiment and theory are found to be $\delta\Delta_{12}=0.018, 0.013$ and 0.012 meV correspondingly. Sample A. Inset shows semi-classical trajectories in k -space at finite in-plane magnetic field B_{\parallel} .

region ($B_{\perp} \in (0.07-0.2)$ T) demonstrate standard deviation below 0.005 T and also deviates systematically from each other near the apex of the $k=3$ region in the range $B_{\perp} \in (0.15-0.2)$ T. The systematic deviations between the experiment and the theory is discussed below, where we present different regimes in detail.

B. Semi-classical regime

The semi-classical regime corresponds to weak perpendicular magnetic fields at which the Landau-Zener transitions (magnetic breakdown) between different semi-classical electron trajectories are exponentially weak and are neglected³⁰. Electrons perform semi-classical motion along trajectories corresponding to the symmetric and antisymmetric states. At $\alpha=0$ ($B_{\parallel}=0$ T) the semi-classical trajectories are circles with the same origin $\vec{k}=0$ in the k -space. At an energy E the symmetric wave function propagates along the circle with a radius $k^S > k^{AS}$ and the gap between two subbands Δ_{12} does not depend on the wave vector \vec{k} .

Application of a parallel field shifts the centers of the two circles by $\delta k = \pm edB_{\parallel}/2\hbar$ leading to variations of the gap between two subbands with \vec{k} .^{29,30} The insert to Figure 6 presents an example of the semi-classical trajectories when a parallel field B_{\parallel} is applied. The semi-

classical trajectory enclosing the gray area corresponds to the symmetric wave function, while the solid line, which is inside the intersection between two circles, presents the trajectory corresponding to the antisymmetric wave function. The frequency of quantum oscillations in the reciprocal magnetic field $1/B_{\perp}$ is proportional to the area enclosed by semi-classical trajectory at an energy E .^{1,3} In the case of HF-MISO the energy E is equal to the energy at the bottom of the third subband: $E = E_3$. The symmetric state, thus, has a frequency f_{31} , which is higher than the frequency of quantum oscillations due to the trajectory of the antisymmetric state f_{32} . The difference between two frequencies f_{12} is proportional to the area A , shown in gray in the insert. In accordance with Eq.(1) at $B_{\parallel}=0$ the gap $\Delta_{12} = 2t_0$ is proportional to f_{12} and, thus, to the area A . An increase of the in-plane field B_{\parallel} further shifts the centers of the two circles increasing the gray area A and, thus, the gap Δ_{12} .

Figure 6 demonstrates the increase of the gap with in-plane magnetic field. Filled (open) symbols present the gap Δ_{12} obtained from the relation $\Delta_{12} = k \cdot \hbar\omega_c$, using experimental positions of LF-MISO maximum (HF-MISO node), where the corresponding index k is an integer (half-integer). Solid lines present the gap obtained from the same relation, using the numerical evaluation of the positions of LF-MISO maximums, which are shown in Fig.5(a). Figure 6 demonstrates good agreement between the numerically evaluated gap and experimental data. The HF-MISO node $k=5/2$ and $k=3$ LF-MISO maximum are clearly seen at high magnetic fields and, thus, the corresponding gaps are presented in a broader range of parallel fields in comparison with the gap obtained from the $k=2$ LF-MISO maximum. The values of experimental and numerical gaps, obtained from the $k=2$ LF-MISO maximum, are found to be larger than those with higher MISO indexes. These results are related to magnetic breakdown of semi-classical trajectories, which is stronger at the $k=2$ LF-maximum.

Figure 6 shows also that the curves corresponding to the numerically evaluated gaps collapse at high indexes k . This collapse is the signature of the semi-classical regime at which magnetic breakdown is nearly absent and, thus, the obtained gap does not depend on the perpendicular magnetic field. The strength of magnetic breakdown is shown in Fig.4. A comparison between Figures 6 and 4 indicates, that for the gap, obtained from the MISO with high indexes k , magnetic breakdown is indeed small at $B_{\parallel} < 0.1$ T. For $k < 3$ the probability of magnetic breakdown increases exceeding 50% for $k=2$ at $B_{\parallel}=0.1$ T and $B_{\perp}=0.27$ T.

Finally we would like to note that the dependence of the gap Δ_{12} on the in-plane field B_{\parallel} , which is shown in Fig.6, is not the dependence of the difference between the bottoms of the symmetric and anti-symmetric bands. As mentioned above the bottom part of the spectrum is weakly affected by B_{\parallel} . In contrast to the case of pure perpendicular magnetic field ($B_{\parallel}=0$ T), a finite parallel magnetic field makes the level spacing energy dependent

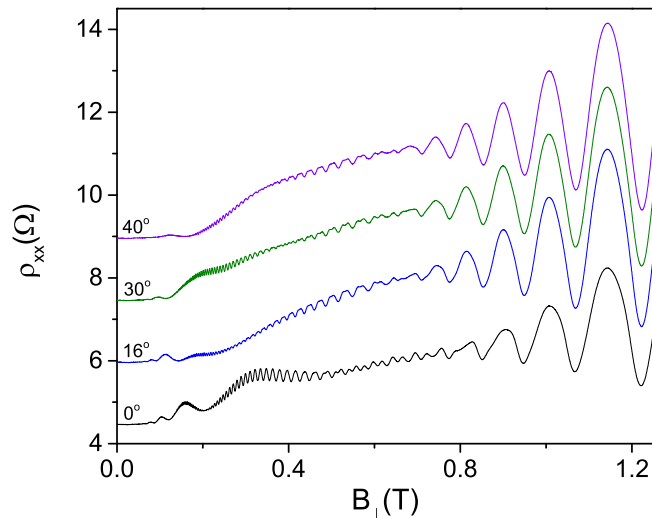


FIG. 7: Magnetoresistance of GaAs quantum well at different angles between the magnetic field and normal to the sample. Three upper curves are shifted for clarity. $T=4.2\text{K}$. Sample B.

and the extracted gap represents the relative position of the symmetric and antisymmetric levels in the vicinity of the Fermi energy.

C. High magnetic field regime

In a strong magnetic field B_{\perp} the cyclotron energy exceeds the gap: $\hbar\omega_c \gg \Delta_{12}$. In this range of magnetic fields Shubnikov de Haas (SdH) oscillations are well developed. Figure 7 presents the magnetoresistance taken at different angles α between the direction of the applied magnetic field and the normal to the 2D sample. At temperature $T=4.2\text{K}$ SdH oscillations appear in B_{\perp} exceeding 0.5T . At a smaller field these oscillations are significantly damped and only MISO are observable at $T=4.2\text{K}$.⁴⁵

The amplitude of SdH oscillations increases considerably with angle. Figure 8 demonstrates the angular dependence of a swing (doubled amplitude) of SdH oscillations taken at $B_{\perp}=1.14\text{T}$. The swing of SdH oscillations is measured between upper and low branches of the envelope of SdH oscillations. The upper (low) branches of the envelope are obtained using a cubic spline between maximums (minimums) of SdH oscillations.⁴⁵ The swing of oscillations increases monotonically from $2.65\ \Omega$ at $\tan(\alpha)=0$ to about $4.35\ \Omega$ at $\tan(\alpha)\approx 0.4$. Then the oscillation swing demonstrates small periodic variations with $\tan(\alpha)$.

To evaluate the SdH amplitude we used the following expression. The SdH amplitude depends on the level spacing δE_l in the vicinity of the Fermi energy since all quantum states below E_F are completely occupied. This fact allows for a modification of the actual distribution of the occupied levels inside subbands to simplify

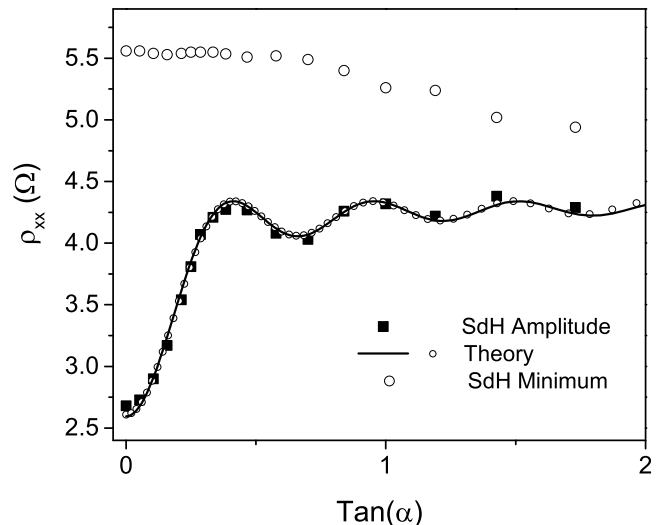


FIG. 8: Dependence of the swing of SdH oscillations at $B_{\perp}=1.14\text{ T}$ on $\tan(\alpha)$. Filled squares present experimental data obtained from the magnetoresistance curves shown in Fig.7 with an accuracy approximated by the size of the symbols. Solid line (small open circles) is a theoretical dependence obtained from numerical (analytical) evaluation of the electron spectrum at fixed $B_{\perp}=1.14\text{ T}$ and different B_{\parallel} corresponding to different angles α using $A_{SdH}=2.17 \pm 0.01\ \Omega$ and $\gamma=0.479 \pm 0.01\ \text{meV}$ as fitting parameters and $t_0=0.215\ \text{meV}$, $d=36\ \text{nm}$ and $E_F=15.1\ \text{meV}$. Big open circles present the angle dependence of the sample resistance in the SdH minimum at $B_{\perp}=1.07\ \text{T}$. $T=4.2\text{K}$. Sample B.

the mathematical description of SdH oscillations. Below we use a level distribution with equal spacing, $\hbar\omega_c$, inside each subband. The two periodic sets of levels are shifted with respect to each other by the value corresponding to the actual spacing δE_l between the nearest quantum levels in the vicinity of the Fermi energy. The spectrum modification doesn't change the number of occupied states preserving the total electron density. The modified spectrum is similar to the spectrum at $B_{\parallel}=0\ \text{T}$ with $\Delta_{12} = \delta E_l$ and yields SdH oscillations approximated by a cosine function:

$$\Delta\rho_{SdH}^{(i)} = A_{SdH}^{(i)} \cos\left(\frac{2\pi(E_F - E_*^{(i)})}{\hbar\omega_c}\right) \quad (5)$$

The SdH amplitude, $A_{SdH}^{(i)}$, includes Dingle factor $d_i = \exp(-\pi/\omega_c\tau_q^{(i)})$ and a temperature damping factor $A_T = x/\sinh(x)$, where $x = 2\pi^2kT/\hbar\omega_c$.¹ In contrast to HF-MISO the phase of the cosine contains the Fermi energy instead of the energy of the bottom of the third subband E_3 (see Eq.(1)). The energy $E_*^{(i)}$ corresponds to the bottom of the modified spectrum of the i th subband. Due to the nearly equal quantum scattering times in the symmetric and antisymmetric subbands both SdH oscillations have the same amplitude A_{SdH} . The sum of the two oscillations $\Delta\rho_{SdH} = \Delta\rho_{SdH}^{(1)} + \Delta\rho_{SdH}^{(2)}$ can be pre-

sented as a product of two cosines:

$$\begin{aligned} \Delta\rho_{SdH} &= 2A_{SdH} \cos\left(\frac{\pi E_+}{\hbar\omega_c}\right) \cos\left(\frac{\pi E_-}{\hbar\omega_c}\right) \\ &\approx 2A_{SdH} \cdot \cos\left(\frac{\pi E_+}{\hbar\omega_c}\right) \left(1 - \frac{1}{2} \left(\frac{E_-}{\gamma}\right)^2\right), \quad (6) \end{aligned}$$

where $E_+ = 2E_F - E_*^{(1)} - E_*^{(2)}$ is the sum and $E_- = E_*^{(2)} - E_*^{(1)}$ is the difference between the energy terms in Eq.(5). The energy E_+ describes the high frequency content of the SdH oscillations, which is intact since both the total electron density and the Landau levels degeneracy $g = 1/(2\pi l_\perp^2)$ are preserved in the modified spectrum. We note also that the difference between the terms equals the actual level spacing near E_F : $E_- = \delta E_l$. Thus Eq.(6) provides a description of SdH oscillations corresponding to the actual spectrum E_l . Since in high magnetic fields the cyclotron energy is considerably higher than the level spacing δE_l the low frequency cosine, modulating the SdH amplitude, is approximated by a Taylor series. At $B_\perp = 1.14$ T the factor $\gamma = \hbar\omega_c/\pi \approx 0.63$ meV is larger than $\Delta_{12} = 0.43$ meV at $B_\parallel = 0$ T.

The approximation of SdH oscillations by a single cosine is valid when the swing of SdH oscillations is small in comparison with the Drude resistance at $B_\perp = 0$ T. In the studied case the oscillation swing is comparable with the Drude resistance and, thus, higher harmonics of SdH oscillations should be accounted for. In the case of a small level spacing between subbands: $E_- \ll \hbar\omega_c$, variations of the amplitude of the higher harmonics with the angle α are expected to be also proportional to E_-^2 similar to the variations of the fundamental harmonic in Eq.(6). Taking this into account we compare the theory and experiment using Eq.(6) with A_{SdH} and γ as fitting parameters.

Shown in Fig.8 the solid line presents the angular dependence of the swing of SdH oscillations yielded by Eq.(6). The energy E_- is extracted from the electron spectra evaluated numerically at fixed $B_\perp = 1.14$ T and different $B_\parallel = B_\perp \tan(\alpha)$. For each combination of B_\perp and B_\parallel the energy spectrum E_l is computed with the same model parameters $t_0 = 0.215$ meV and $d = 36$ nm used in previous spectrum computations shown Fig.4-6. The standard deviation between the experimental data and the numerical evaluation of the SdH amplitude is found within 0.05Ω indicating a good agreement between the experiment and the proposed model.

Shown in Fig.8 the small open circles present a theoretical dependence obtained from the analytical expression for the level spacing in high magnetic fields: $\delta E_N = 2t_0 \exp(-\theta) L_N(2\theta^2)$, where $\theta = B_\parallel d / (2B_\perp l_\perp)$.³⁰ At high N the Laguerre function, $L_N(x)$, is approximated by a Bessel function, $J_0(x)$, yielding the level spacing $E_- = \delta E_l \approx 2t_0 J_0[k_F d \tan(\alpha)]$, where $k_F = (2mE_F)^{1/2}$ is wave number at the Fermi energy. The analytical evaluation of the swing of SdH oscillations demonstrates better agreement with the numerical data yielding the standard deviation within 0.01Ω . The results indicate that

the inaccuracy of the numerical computations of the electron spectrum is likely not the main source of the deviations between the experiment and theory.

Fig.8 demonstrates oscillations and the complete reduction of the tunneling magnitude in the maximums of the oscillations. At an angle α_n corresponding to n -th maximum, the beating pattern between two SdH oscillations is absent since the beating period ($\sim 1/E_-$) is infinite at the angle α_n . The absence of the beating pattern at "magic angles" as well as the beating of SdH oscillations is observed in strongly anisotropic layered organic materials.^{50,51} These resistance oscillations with the angle α in high magnetic fields have been seen recently in double quantum wells in the Quantum Hall effect regime.^{39,40}

The evolution of the level spacing with the angle α can be understood using an intuitively appealing picture of the phenomenon.^{52,53} In the bilayer geometry the tunneling between layers a and b can be described by the Hamiltonian

$$H_t = t_0 \int \phi_a^*(\mathbf{r}) \phi_b(\mathbf{r}) \exp(i e A_z(\mathbf{r}) d / \hbar) d^2 r + H.c., \quad (7)$$

where vector potential $A_z = B_\parallel x$ corresponds to the in-plane magnetic field directed along y -axes: $\vec{B} = (0, -B_\parallel, 0)$. In the presence of B_\perp , an electron with Fermi energy propagates along the cyclotron orbit with radius r_c . The gauge phase in Eq.(8) oscillates along the electron trajectory leading to a modification of the tunneling. The effective tunneling amplitude t is obtained by the phase averaging⁵²:

$$t = t_0 \langle \exp(i e B_\parallel x(t) d / \hbar) \rangle_t = t_0 J_0(k_F d \tan(\alpha)). \quad (8)$$

The brackets represent a time average over the period of the cyclotron motion and $x(t) = r_c \cos(\omega_c t)$ is the x -coordinate of the electron. The obtained expression coincides with the one used for fitting experiment data in Fig.8.

In Fig.8 large open circles represent the dependence of the resistance, R_{min} , in the SdH minimum at $B_\perp = 1.07$ T on the in-plane magnetic field. The notable feature of the observed behavior is the stability of the resistance value in a broad range of α despite the significant variations of the SdH amplitude in the same angular range. The stability is found for all other SdH minimums shown in Fig.7. The resistance R_{min} starts to decrease with the angle after the level spacing E_- reaches the first maximum at a finite B_\parallel . In contrast to the SdH amplitude the R_{min} depends on the behavior of the non-oscillating background which was beyond the scope of this paper.

Finally we would like to mention that in the studied samples SdH oscillations are comparable with MISO near $B_\perp \approx 0.5$ T in the vicinity of the HF-MISO node $k=1/2$ shown in Fig.4.⁴⁵ The presence of SdH oscillations may affect the position of this node since the phase of SdH oscillations is shifted by π with respect to the phase of MISO^{18,27,45,54}. An analysis of the beating of quantum

oscillations indicates that the nodes of both SdH oscillations and HF-MISO occur at the same magnetic field. In accordance with numerical computation the node $k=1/2$ occurs at $B_{\perp}=0.5\text{T}$. If at $B_{\perp}=0.5\text{T}$ the SdH amplitude is larger than the amplitude of HF-MISO, then the SdH oscillations dominate at $B_{\perp} > 0.5\text{T}$ since the oscillations grow faster than MISO due to the additional temperature factor $A_T(B_{\perp})$ (see Eq.(5)). At $B_{\perp} < 0.5\text{T}$ the SdH oscillations are comparable with HF-MISO and the destructive interference between two oscillations reduces the overall oscillation amplitude. It makes the actual node to be broader and shifted toward smaller magnetic fields. This is indeed seen in Fig.4 near the $k=1/2$ node. We suggest that the systematic deviation between experiment and the theory observed at the $k=1/2$ node is the result of destructive interference between SdH oscillations and MISO.

D. Magnetic breakdown regime

As mentioned above an application of parallel field, B_{\parallel} , shifts the centers of cyclotron orbits in two layers by $\delta k = \pm edB_{\parallel}/2\hbar$ leading to variations of the gap between the two subbands with \vec{k} .^{29,30} The smallest gap occurs in a small region with lateral size $\Delta k_0(B_{\parallel})$ near the intersections between two circles shown in the insert to Fig.6. At small magnetic fields electrons circulate along the semi-classical trajectories $\vec{k}_S(t)$ and $\vec{k}_{AS}(t)$, corresponding to the symmetric and antisymmetric states. The probability of magnetic breakdown between these trajectories depends strongly on the time Δt during which electrons pass the region with the smallest gap: $\Delta t \sim \hbar\Delta k_0/eV_F B_{\perp}$. At small magnetic fields the time $\Delta t \gg \hbar/t_0$ is long enough to establish the gap between subbands and magnetic breakdown is exponentially suppressed.³²⁻³⁴ An increase of both B_{\perp} and B_{\parallel} increases the probability of magnetic breakdown. In a WKB approximation an expression has been obtained for the breakdown probability P_{MB} ³⁰:

$$P_{MB} = \exp(-\omega_c^*/\omega_c), \quad (9)$$

where

$$\omega_c^* = \frac{\pi t_0^2}{E_F(Q/k_F)[1 - (Q/2k_F)^2]^{1/2}}. \quad (10)$$

Here $Q = deB_{\parallel}/\hbar$ is the relative displacement of the two Fermi circles due to B_{\parallel} .

The 50% probability of the magnetic breakdown at different B_{\perp} and B_{\parallel} is plotted in Fig.4 for sample A. Fig.4 demonstrates a correlation of magnetic breakdown with the behavior of the nodal lines. In particular the collapse of 5/2 and 7/2 nodes occurs at a higher B_{\parallel} than the one of 1/2 and 3/2 nodes that is in qualitative agreement with the behavior of the line describing magnetic breakdown.

The notable feature of magnetic breakdown is the growth of quantum oscillations with frequency equal to

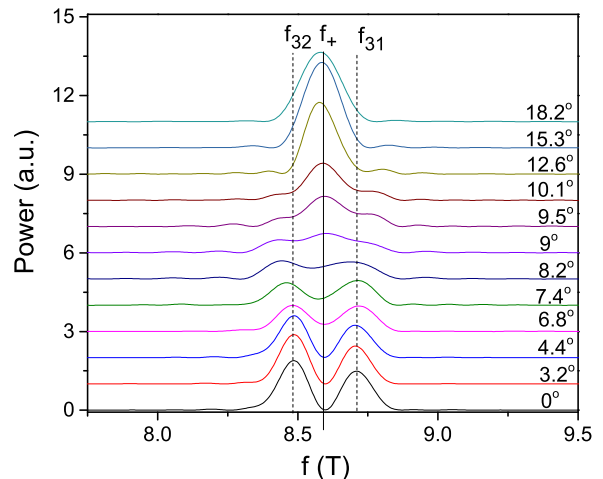


FIG. 9: Fourier power spectra of MISO at different angles as labeled. The spectra are obtained in the interval of reciprocal magnetic fields between 2 and 10 1/T shown in Fig.2. The spectra are vertically shifted for clarity. Sample A.

half sum of the frequencies corresponding to symmetric and antisymmetric semi-classical trajectories: $f_+ = (f_{31} + f_{32})/2$.^{30,37,55} The frequency, f_+ , is due to the circular orbital motion of an electron completely located in one of the layers. The following consideration helps to understand the origin of the frequency f_+ . In accordance with Eq.(9) at small B_{\perp} : $\omega_c \ll \omega_c^*$ the probability of magnetic breakdown is exponentially small and, thus, can be neglected. In the absence of magnetic breakdown electrons follow the semi-classical trajectories and the spectrum of the quantum oscillations contains frequencies $f_S = f_{31}$ and $f_{AS} = f_{32}$ corresponding to the symmetric and antisymmetric subbands. An example of the semi-classical trajectories corresponding to the two subbands in a finite B_{\parallel} is shown in the insert to Fig.6. Following the semi-classical trajectory an electron moves periodically between the top and bottom layers. An increase of the perpendicular magnetic field enhances the probability of magnetic breakdown. At $\omega_c > \omega_c^*$ the electron has a considerable probability to cross the tunneling gap and to follow a trajectory, which is not perturbed by the tunneling. This trajectory is a circular orbit located completely in a single layer. These orbits are presented by dashed lines in the insert to Fig.6. The insert indicates that the total area of the two circles equals the sum of the area inside the perimeter of the shifted circles (symmetric subband) and the area of the overlap of the two circles (antisymmetric subband). Since the frequencies of the quantum oscillations are proportional to the corresponding areas¹ the relation between different areas yields: $2f_+ = (f_{31} + f_{32})$.

Figure 9 shows the increase of the amplitude of quantum oscillations with frequency f_+ as magnetic breakdown increases. At zero angle α magnetic breakdown is absent and the spectrum of MISO contains only two frequencies f_{31} and f_{32} corresponding to symmetric and

antisymmetric subbands. With an increase of α the magnitude of parallel magnetic field and, thus, the probability of magnetic breakdown increase. The enhanced magnetic breakdown decreases the magnitude of MISO and increases the magnitude of the oscillations corresponding to the isolated 2D layers, which appear at frequency $f_+ \approx (f_{31} + f_{32})/2$. At $\alpha > 13^\circ$ the oscillations at frequency f_+ are predominant.

Figure 9 demonstrates also an increase of the difference between frequencies f_{31} and f_{32} corresponding to symmetric and antisymmetric subbands with the angle α . The increase of $\Delta f = f_{31} - f_{32}$ is related to the increase (decrease) in size of the symmetric (antisymmetric) orbits with the increase of in-plane magnetic field²⁹.

Magnetic breakdown is the origin of the collapse of HF-MISO nodes and the nodal confinement of LF-MISO with odd indexes k as shown in Fig.4. To understand this relation we note that the phase of the oscillations with frequency f_+ is the same as the phase of HF-MISO for even k and is shifted by π for odd k . Fig.2 shows this correspondence: in the $k=1$ region maximums of HF-MISO at $\alpha=0^\circ$ (no magnetic breakdown) correspond to minimums of HF-MISO at $\alpha=15.3^\circ$ (strong magnetic breakdown), while in the $k=2$ region these two HF-MISOs are in-phase. Magnetic breakdown admixes oscillations similar to one at $\alpha=15.3^\circ$ to the oscillations at $\alpha=0^\circ$, and, therefore, decreases the magnitude of the oscillations corresponding to the odd k . Thus, the magnitudes of odd k HF-MISO and corresponding LF-MISO maximum decrease.

The mixing moves the nodes, confining an odd k region, toward each other. The insert to Fig.10 presents a phasor diagram illustrating this property. Eq.(1) describes MISOs corresponding to symmetric and antisymmetric subbands by cosine functions with frequencies $f_{3i} \sim \Delta_{3i}$. Shown in the insert two vectors \vec{A}_S and \vec{A}_{AS} represent the amplitude and phase of the two cosine functions corresponding to symmetric and antisymmetric subbands. Without magnetic breakdown the two oscillations are in phase and, thus, the two vectors are in the same direction at HF-MISO antinodes. Below we consider the $k=1$ region. As shown in Fig.2 the $k=1$ antinode occurs at $1/B_\perp^{an} \approx 4$ 1/T. A right shift of the $1/B_\perp$ to the nearest node $k=3/2$, located at $1/B_\perp^n \approx 6$ 1/T, destroys the parallel alignment between the two vectors. In a reference frame rotating with frequency f_+ the right shift rotates the vector \vec{A}_S (\vec{A}_{AS}) counter clockwise (clockwise) yielding a phase angle π between two vectors, that corresponds to an orientation of two vectors in opposite directions. At the node the sum of the vectors is zero that corresponds to the completely destructive interference between the two oscillations.

Magnetic breakdown adds an additional vector, \vec{A}_{MB} , to the phasor diagram. The amplitude of \vec{A}_{MB} corresponds to the amplitude of the quantum oscillations at frequency f_+ . To simplify the presentation we use the magnitude of the vector \vec{A}_{MB} to be the same as the other

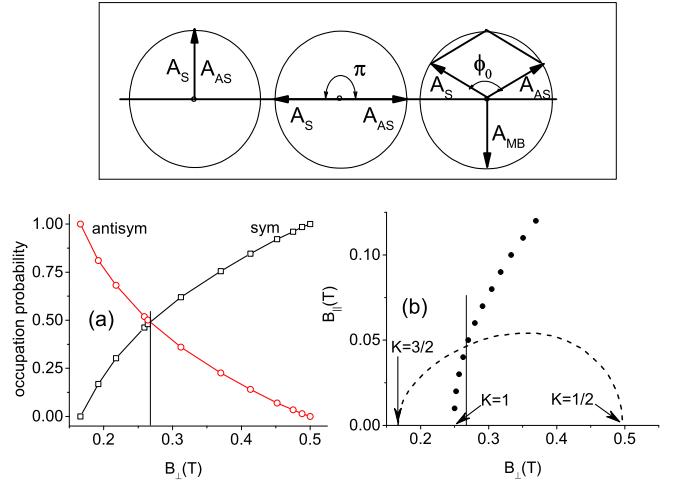


FIG. 10: (a) Open symbols present contributions of symmetric and antisymmetric states to population of quantum level $|l\rangle = c_S|S\rangle + c_{AS}|AS\rangle$ in the vicinity of Fermi energy at different B_\perp and B_\parallel corresponding to the nodal line shown in (b). The eigenstate $|l\rangle$ of the Hamiltonian \hat{H} is computed numerically; (b) Dashed line presents nodal line enclosing the $k=1$ region. Solid symbols show positions of level $|l\rangle = (|S\rangle + |AS\rangle)/\sqrt{2}$ with the equal population of the symmetric and antisymmetric states in $B_\perp - B_\parallel$ plane. The dependence intersects the nodal line at the same magnetic field B_\perp at which two lines shown in (a) intersect. Sample A. Insert shows phasor diagram describing interference of MISOs presented by \vec{A}_S and \vec{A}_{AS} with quantum oscillations, \vec{A}_{MB} , induced by magnetic breakdown.

magnitudes. In the rotating frame the vector \vec{A}_{MB} is oriented down since in odd k regions the phase of oscillations, induced by magnetic breakdown, is shifted by π with respect to the MISO phase at the antinode. In the magnetic breakdown regime the node occurs at a phase difference ϕ_0 between \vec{A}_S and \vec{A}_{AS} , at which the sum of three vectors $\vec{A}_S + \vec{A}_{AS} + \vec{A}_{MB}$ is zero. The angle ϕ_0 is smaller than π and, thus, corresponds to a node located at $1/B_\perp^{MB} < 1/B_\perp^n$ closer to the antinode position at $1/B_\perp^{an}$. At a larger magnitude A_{MB} the angle ϕ_0 is smaller indicating further displacement of the node position toward the antinode. A similar consideration of the $k=1/2$ node shows the node displacement in the opposite direction i.e. again toward the antinode at $1/B_\perp^{an} \approx 4$ 1/T. Finally at $|\vec{A}_{MB}| = |\vec{A}_S| + |\vec{A}_{AS}|$ the phase difference $\phi_0=0$ and the two nodes collapse bounding completely the $k=1$ region in the $B_\perp - B_\parallel$ plane.

Below we consider additional properties of the $k=1$ region and the nodal line between $k=1/2$ and $k=3/2$ nodes. Figure 10 demonstrates the probabilities of the population of the symmetric and antisymmetric states along the nodal line for a quantum state $|l\rangle$ in the vicinity of the Fermi energy. The probabilities are obtained from an analysis of the eigenvectors of the Hamiltonian \hat{H} (see Eq.(3) and Eq.(4)). The numerical computations indicate that at the nodal line the eigenvector $|l\rangle$ contains

primarily the contributions from one symmetric and one antisymmetric state: $|l\rangle \approx c_S|S\rangle + c_{AS}|AS\rangle$, where c_A and c_{AS} are the amplitude of the states. All other contributions to the level population are within a few percents and are neglected.

Fig.10(a) presents the probability $P_S = c_S^2$ and $P_{AS} = c_{AS}^2$ at different B_\perp and B_\parallel corresponding to the nodal line around the $k=1$ region. The figure demonstrates that at the node $k=3/2$ located at $B_\perp=0.166$ T and $B_\parallel=0$ T the quantum state $|l\rangle$ is completely antisymmetric: $c_S=0$ and $c_{AS}=1$. This node is due to the interlayer tunneling only. A shift along the nodal line increases both B_\perp and B_\parallel enhancing the magnetic breakdown, which in turn increases (decreases) the population of the symmetric (antisymmetric) states. At $B_\perp=0.268$ T the two states are equally populated and $|l\rangle = (|S\rangle \pm |AS\rangle)/\sqrt{2}$. Fig.10(b) indicates that an approach of B_\perp to the $k=1/2$ node decreases B_\parallel and the magnetic breakdown. Finally at the node $k=1/2$ located at $B_\perp=0.5$ T and $B_\parallel=0$ T the probability of magnetic breakdown is zero and the state $|l\rangle$ is formed again by the interlayer tunneling only. However in contrast to the state $|l\rangle$ at $k=3/2$ the state $|l\rangle$ is now completely symmetric. The transformation of the state symmetry occurs while the state $|l\rangle$ was always gapped since at a nodal line the energy levels are evenly spaced by $\hbar\omega_c/2$.

The observed smooth transformation of the level symmetry is due to a repulsion of the quantum levels induced by magnetic breakdown. Without the magnetic breakdown at $B_\parallel=0$ T the symmetry of the state $|l\rangle$ changes abruptly with the perpendicular magnetic field at $B_\perp=0.25$ T corresponding to the $k=1$ LF-MISO maximum. At this magnetic field the energies of $|N+1, S\rangle$ and $|N, AS\rangle$ states of the symmetric and antisymmetric bands coincide and, thus, the gap between these levels is zero. At $B_\perp=0.25$ T and $B_\parallel=0$ T these two levels cross each other. Magnetic breakdown opens up a gap between the levels leading to a smooth transformation of the symmetry of the eigenvector $|l\rangle$. The solid symbols show locations of the quantum level with equal symmetric and antisymmetric population $|l_{eq}\rangle = (|S\rangle + |AS\rangle)/\sqrt{2}$. The line divides the area under the nodal line on the symmetric and antisymmetric parts. At high B_\parallel the location of the level $|l_{eq}\rangle$ approaches the location of the $k=2$ LF-MISO maximum (not shown).

We note that near $B_\perp=0.25$ T and $B_\parallel=0$ T the numerical simulations show a substantial increase of the level splitting for small magnetic breakdown between the two states indicating a strong sensitivity of the electron spectrum to the parallel magnetic field at $k=1$. Such strong sensitivity of the spectrum to the B_\parallel is also seen in the perturbation expansion of the spectrum vs $B_\parallel d/2B_\perp l_\perp$.³⁰ Eq.(4.7) of the paper³⁰ indicates a divergence of the second order correction to the level spacing δE_l at $\hbar\omega_c = 2t_0$ corresponding to the $k=1$ MISO maximum. These results agree with the presented experiments demonstrating significant sensitivity of the MISO maximum at $k=1$ to in-plane magnetic field.

Finally we would like to discuss the discrepancy between experimental and theoretical positions of the HF-MISO node, which is observed near the apexes of the odd regions $k=3$ and $k=5$, where nodal lines ($k \pm 1/2$) meet each other in Fig.4. This discrepancy is not related to SdH oscillations since the SdH amplitude is negligibly small at these magnetic fields⁴⁵. Figure 4 demonstrates that the probability of the magnetic breakdown near the apexes is 50%. Numerical computations reveal that, near these apexes the eigenstate of the studied Hamiltonian \hat{H} contains comparable contributions from symmetric and antisymmetric quantum states of many Landau levels. Thus the quantum state possesses a complex set of semiclassical trajectories. In general different trajectories provide different contributions to the transport^{30,34-36}. This property of the quantum states has not been taken into account in the presented model. We suggest that the observed deviations between experiment and theory are related to the complex structure of quantum levels near the apexes of odd k regions. The complex structure is induced by magnetic breakdown.

IV. CONCLUSION

Magneto-inter-subband oscillations of the resistance of two dimensional electrons are investigated in wide GaAs quantum well with three populated subbands placed in tilted magnetic fields. At zero in-plane magnetic field the oscillations demonstrate three distinct frequencies $f_{ij} \sim \Delta_{ij}$ in reciprocal perpendicular magnetic field $1/B_\perp$. The low frequency oscillations, LF-MISO, is due to enhancement of the electron scattering when Landau levels of two lowest, symmetric and antisymmetric subbands, are aligned with each other. These oscillations obey the relation: $\Delta_{21} = k \cdot \hbar\omega_c$. Related to the third subband two HF-MISOs have much higher frequencies: f_{31} and f_{32} due to the higher energy difference between bottoms of the third and lowest subbands: $\Delta_{3i} \gg \Delta_{21}$. HF-MISOs demonstrate a distinct beating pattern with a beat frequency $f_{beat} = (f_{31} - f_{32})/2$. A rotation of the direction of the magnetic field by an angle α from the normal to the samples produces dramatic changes of MISO. At small α the LF-MISO maximum and the corresponding antinode of HF-MISO at $k=1$ disappear. In the $B_\perp - B_\parallel$ plane the $k=1$ region is found to be bounded by a continuous nodal line connecting the $k=3/2$ and $k=1/2$ nodes of HF-MISO. Similar nodal bounding is found for other odd k regions. This bounding correlates with the probability of magnetic breakdown, P , between semiclassical trajectories corresponding to symmetric and antisymmetric subbands. The nodal bounding is mostly completed at $P < 1/2$ for $k=1$ and $k=3$ regions. The Fourier analysis of the oscillations beyond the bounded regions shows the dominant contribution of the oscillations to be of period $f_+ = (f_{31} + f_{32})/2$ corresponding to the electron orbits located at either side of the quantum well and populated by magnetic breakdown. The loca-

tion of the HF-MISO nodes as well as the evolution of the LF-MISO maximum on $B_{\perp} - B_{\parallel}$ plane are found to be in an excellent agreement with numerical evaluations of the electron spectra.

Authors thank Scott Dietrich for help with experi-

ments. This work was supported by the National Science Foundation (Division of Material Research - 1104503), the Russian Foundation for Basic Research (project no.16-02-00592) and the Ministry of Education and Science of the Russian Federation.

-
- * Corresponding author: vitkalov@sci.ccnyc.cuny.edu
- ¹ D. Shoenberg *Magnetic oscillations in metals*, (Cambridge University Press, 1984).
 - ² T. Ando, A. B. Fowler, and F. Stern, *Rev. of Mod. Phys.* **B 54**, 437 (1982).
 - ³ J. M. Ziman *Principles of the theory of solids*, (Cambridge at the University Press, 1972).
 - ⁴ Sankar D. Sarma, Aron Pinczuk *Perspectives in Quantum Hall Effects*, (Wiley-VCH, Weinheim, 2004).
 - ⁵ I. A. Dmitriev, M.G. Vavilov, I. L. Aleiner, A. D. Mirlin, and D. G. Polyakov, *Phys. Rev. B* **71**, 115316 (2005).
 - ⁶ Jing-qiao Zhang, Sergey Vitkalov, A. A. Bykov, A. K. Kalagin, and A. K. Bakarov *Phys. Rev. B* **75**, 081305(R) (2007).
 - ⁷ Jing Qiao Zhang, Sergey Vitkalov, and A. A. Bykov *Phys. Rev. B* **80**, 045310 (2009).
 - ⁸ N. C. Mamani, G. M. Gusev, O. E. Raichev, T. E. Lamas, and A. K. Bakarov, *Phys. Rev. B* **80**, 075308 (2009).
 - ⁹ A. A. Bykov, Jing-qiao Zhang, Sergey Vitkalov, A. K. Kalagin, and A. K. Bakarov *Phys. Rev. Lett.* **99**, 116801 (2007).
 - ¹⁰ W. Zhang, M. A. Zudov, L.N. Pfeiffer, and K.W. West, *Phys. Rev. Lett.* **100**, 036805 (2008).
 - ¹¹ G. M. Gusev, S. Wiedmann, O. E. Raichev, A. K. Bakarov, and J. C. Portal *Phys. Rev. B* **83**, 041306 (2011).
 - ¹² A. A. Bykov, Sean Byrnes, Scott Dietrich, Sergey Vitkalov, I. V. Marchishin and D. V. Dmitriev, *Phys. Rev. B* **87**, 081409(R) (2013).
 - ¹³ N. R. Kalmanovitz, A. A. Bykov, S. Vitkalov, and A. I. Toropov *Phys. Rev. B* **78**, 085306 (2008).
 - ¹⁴ I. A. Dmitriev, A. D. Mirlin, D. G. Polyakov, M. A. Zudov, *Rev. Mod. Phys.* **84**, 1709 (2012).
 - ¹⁵ M. A. Zudov, R. R. Du, J. A. Simmons and J. R. Reno, *Phys. Rev. B* **64**, 201311(R) (2001).
 - ¹⁶ P. D. Ye, L. W. Engel, D. C. Tsui, J. A. Simmons, J. R. Wendt, G. A. Vawter and J. L. Reno, *Appl. Phys. Lett.* **79**, 2193 (2001).
 - ¹⁷ P. T. Coleridge, *Semicond. Sci. Technol.* **5**, 961 (1990).
 - ¹⁸ D. R. Leadley, R. Fletcher, R. J. Nicholas, F. Tao, C. T. Foxon, and J. J. Harris, *Phys. Rev. B* **46**, 12439 (1992).
 - ¹⁹ A. A. Bykov, D. R. Islamov, A. V. Goran, A. I. Toropov, *JETP Lett.* **87**, 477 (2008).
 - ²⁰ A. A. Bykov, *JETP Lett.* **88**, 64 (2008).
 - ²¹ A. A. Bykov, *JETP Lett.* **88**, 394 (2008).
 - ²² N. C. Mamani, G. M. Gusev, T. E. Lamas, A. K. Bakarov, O. E. Raichev, *Phys. Rev. B* **77**, 205327 (2008).
 - ²³ A. A. Bykov, *JETP Lett.* **89**, 461 (2009).
 - ²⁴ A. V. Goran, A. A. Bykov, A.I. Toropov, S. A. Vitkalov, *Phys. Rev. B* **80**, 193305 (2009).
 - ²⁵ L. I. Magarill and A. A. Romanov, *Sov. Phys. Solid State* **13**, 828 (1971).
 - ²⁶ V. M. Polyakovskii, *Sov. Phys. Semicond.* **22**, 1408 (1988).
 - ²⁷ M. E. Raikh, T. V. Shahbazyan, *Phys. Rev. B* **49**, 5531 (1994).
 - ²⁸ O. E. Raichev, *Phys. Rev. B* **78**, 125304 (2008).
 - ²⁹ G. S. Boebinger, A. Passner, L. N. Pfeiffer, and K. W. West, *Phys. Rev. B* **43**, 12673 (1991).
 - ³⁰ J. Hu and A. H. MacDonald, *Phys. Rev. B* **46**, 12554 (1992).
 - ³¹ M. G. Priestley *Proc. Roy. Soc. A* **276**, 258 (1963).
 - ³² M. H. Cohen, L. Falicov, *Phys. Rev. Lett.* **7**, 231 (1961).
 - ³³ E. I. Blount, *Phys. Rev.* **126**, 1636 (1962).
 - ³⁴ A. A. Slutskin, *Sov. Phys. JETP* **26**, 474 (1968).
 - ³⁵ A. B. Pippard, *Proc. Roy. Soc. A* **270**, 1 (1962).
 - ³⁶ A. B. Pippard, *Phil. Trans. Roy. Soc. A* **256**, 317 (1964).
 - ³⁷ N. E. Harff, J. A. Simmons, S. K. Lyo, and J. F. Klem, G. S. Boebinger, L. N. Pfeiffer, and K. W. West, *Phys. Rev. B* **55**, R13405 (1997).
 - ³⁸ M. A. Mueed, D. Kamburov, M. Shayegan, L. N. Pfeiffer, K.W. West, K.W. Baldwin, and R. Winkler, *Phys. Rev. Lett.* **114**, 236404 (2015).
 - ³⁹ G. M. Gusev, A. K. Bakarov, T. E. Lamas and J. C. Portal, *Phys. Rev. Lett.* **99**, 126804 (2007).
 - ⁴⁰ G. M. Gusev, C. A. Duarte, T. E. Lamas, A. K. Bakarov and J. C. Portal, *Phys. Rev. B* **78**, 155320 (2008).
 - ⁴¹ N. Kumada, K. Iwata, K. Tagashira, Y. Shimoda, K. Muraki, Y. Hirayama, and A. Sawada *Phys. Rev. B* **77**, 155324 (2008).
 - ⁴² V. V. Solovyev, S. Schmult, W. Dietsche, and I. V. Kukushkin, *Phys. Rev. B* **80**, 241310 (2009).
 - ⁴³ J. Nuebler, B. Friess, V. Umansky, B. Rosenow, M. Heiblum, K. von Klitzing, and J. Smet, *Phys. Rev. Lett.* **108**, 046804 (2012).
 - ⁴⁴ S. Wiedmann, G. M. Gusev, O. E. Raichev, A. K. Bakarov, and J. C. Portal, *Phys. Rev. B* **82** 165333 (2010).
 - ⁴⁵ Scott Dietrich, Jesse Kanter, William Mayer, Sergey Vitkalov, D. V. Dmitriev and A. A. Bykov, *Phys. Rev. B* **92**, 155411 (2015).
 - ⁴⁶ M. G. Vavilov and I. L. Aleiner, *Phys. Rev. B* **69**, 035303 (2004).
 - ⁴⁷ Scott Dietrich, S. A. Vitkalov, D. V. Dmitriev, and A. A. Bykov, *Phys. Rev. B* **85**, 115312 (2012).
 - ⁴⁸ The standard deviation δy between two correlated data sets, y_i and y_i^0 is computed using the following formula:
$$\delta y = \left(\sum_{i=1}^N (y_i - y_i^0)^2 / N \right)^{1/2}$$
, where N is number of data points in each set and integer i correlates the data.
 - ⁴⁹ The theory does not depend on the orientation of the B_{\parallel} in the $x - y$ plane of the 2D layers. To keep notations to be consistent with the published results^{30,41} we use B_{\parallel} directed along the electric current (x -direction) in numerical evaluations of the electron spectrum.
 - ⁵⁰ J. Wosnitzer *Fermi Surfaces of Low Dimensional Organic Metals and Superconductors*, (Springer, Berlin, 1996).
 - ⁵¹ T. Ishiguro, K. Yamaji, and G. Saito *Organic Superconductors*, 2nd ed. (Springer, Berlin, 1998).
 - ⁵² Perez Moses and Ross H. McKenzie, *Phys. Rev. B* **60**, 7998

- (1999).
- ⁵³ Victor M. Yakovenko, Benjamin K. Cooper, *Physica E*, **34**, 128 (2006).
- ⁵⁴ T. H. Sander, S. N. Holmes, J. J. Harris, D. K. Maude, and J. C. Portal, *Phys. Rev. B* **58**, 13856 (1998).
- ⁵⁵ A similar frequency is observed in paper⁵⁶. The frequency
- is related to a magnetic breakdown between heavy and light heavy holes, which is induced by a mechanical strain applied to GaAs samples.
- ⁵⁶ J. Shabani, M. Shayegan, and R. Winkler, *Phys. Rev. Lett.* **100**, 096803 (2008).